

**Local structural disorder and superconductivity in  $K_x\text{Fe}_{2-y}\text{Se}_2$** Hyejin Ryu (류혜진),<sup>1</sup> Hechang Lei (雷和畅),<sup>1</sup> A. I. Frenkel,<sup>2,\*</sup> and C. Petrovic<sup>1,†</sup><sup>1</sup>*Condensed Matter Physics and Materials Science Department, Brookhaven National Laboratory, Upton, New York 11973, USA*<sup>2</sup>*Department of Physics, Yeshiva University, New York, New York 10016, USA*

(Received 23 November 2011; revised manuscript received 22 February 2012; published 13 June 2012)

We report significantly enhanced magnetic moment in  $K_{0.69(2)}\text{Fe}_{1.45(1)}\text{Se}_{2.00(1)}$  single crystals with sharp  $T_c$  and bulk superconductivity obtained by postannealing and quenching process. There are two Fe sites in the  $K_{0.69(2)}\text{Fe}_{1.45(1)}\text{Se}_{2.00(1)}$  unit cell: Fe1, which has higher symmetry with longer average Fe-Se bond length, and Fe2, which has lower symmetry with shorter average Fe-Se bond length. Temperature-dependent x-ray absorption fine-structure (XAFS) analysis results on quenched and as-grown  $K_{0.69(2)}\text{Fe}_{1.45(1)}\text{Se}_{2.00(1)}$  crystals show that quenched  $K_{0.69(2)}\text{Fe}_{1.45(1)}\text{Se}_{2.00(1)}$  have increased average Fe-Se bond length and decreased static disorder. Our results indicate that nonzero population of Fe1 sites is the key structural parameter that governs the bulk superconductivity. We also show clear evidence that Fe1 sites carry higher magnetic moment than Fe2 sites.

DOI: [10.1103/PhysRevB.85.224515](https://doi.org/10.1103/PhysRevB.85.224515)

PACS number(s): 74.62.Bf, 74.25.Ha, 74.62.En, 78.70.Dm

**I. INTRODUCTION**

The discovery of superconductivity in  $\text{LaOFeAs}_{1-x}\text{F}$  with transition temperature  $T_c$  up to 26 K stimulated a variety of studies on iron based superconductors.<sup>1</sup> The  $T_c$  in arsenides was soon raised up to 55 K and was also discovered in simple binary structures of selenide materials,  $\text{FeSe}$ ,<sup>2</sup>  $\text{FeTe}_{1-x}\text{Se}_x$ ,<sup>3</sup> and  $\text{FeTe}_{1-x}\text{S}_x$ ,<sup>4</sup> that do not have any crystallographic layer in between puckered Fe-Se(Te) sheets.  $\text{FeSe}$  is easily affected by pressure since the  $T_c$  can be increased from 8 to 37 K with  $dT_c/dP \sim 9.1$  K/GPa. One possible explanation for this behavior is the empirical rule that the  $T_c$  correlates with the anion height between Fe and Se layers, with an optimal distance around 0.138 nm for maximum  $T_c \sim 55$  K.<sup>5</sup> Recently, the superconducting  $T_c$  was enhanced to above 30 K in iron selenide material not by external pressure but by intercalating alkaline metal (K) between the  $\text{FeSe}$  layers (AF $\text{FeSe}$ -122 type).<sup>6</sup> In addition, it is reported that the superconducting state can be obtained from an insulating state by postannealing and fast quenching.<sup>7</sup>

In this work, we have exploited Fe and Se  $K$ -edge spectra using x-ray-absorption fine structure (XAFS) of as-grown and quenched  $K_{0.69(2)}\text{Fe}_{1.45(1)}\text{Se}_{2.00(1)}$  in order to examine the local lattice and electronic structure around the Fe and Se atoms. We show strong evidence that superconducting volume fraction increase is intimately connected with the increased occupancy of the high-symmetry Fe site, accompanied by the increased average Fe-Se distance and decreased average configurational (static) disorder in this distance.

**II. EXPERIMENT**

As-grown and quenched  $K_{0.69(2)}\text{Fe}_{1.45(1)}\text{Se}_{2.00(1)}$  single crystals were prepared as described previously.<sup>8,9</sup> X-ray-absorption experiments were completed at beamline X19A of the National Synchrotron Light Source. Temperature-dependent x-ray-absorption data were collected in the transmission mode. Gas-filled ionization chamber detectors were used for incident, transmitted, and reference channels. A closed-cycle He cryostat was used to cool the samples with temperature control within  $\pm 1$  K. A minimum of two scans were measured for each temperature for optimal signal-to-

noise ratio. All XAFS spectra were analyzed using the ATHENA and ARTEMIS software programs.<sup>10</sup>

We compared several different modeling schemes in fitting FEFF6 theory to the experimental data in order to obtain structural information from XAFS analysis. The models compared were (1) the multiple edge model, where we varied Fe and Se edge data concurrently by constraining their bond lengths and their disorders to be the same at each temperature, (2) the model where we added a third cumulant to the Fe-Se contribution of each data set, (3) the multiple data set model where we constrained the disorder parameter to follow the Einstein model with static disorder (vide infra), and (4) the model where we added a Fe-Fe contribution to the Fe edge fits. After comparing the fit qualities and inspecting the best-fit results for their physical meaning, we chose model (3) for presenting our results, although the main trends in the results remained the same across all models we tried. We found that adding a third cumulant to the final fit model did not change the results within the error bars, and the best-fit values of the third cumulant were consistent with zero.

**III. RESULTS AND DISCUSSION**

The superconducting volume fractions at 1.8 K of  $K_{0.69(2)}\text{Fe}_{1.45(1)}\text{Se}_{2.00(1)}$  crystals increased by annealing and quenching process from  $\sim 74.6\%$  to  $\sim 87.9\%$  [Fig. 1(a)]. Moreover, the superconductivity in the quenched sample is more homogeneous and sharper at  $T_c \sim 30$  K than in as-grown samples [Fig. 1(a)]. In addition, there is a significant enhancement of susceptibility in the normal state after the postannealing and quenching process [Fig. 1(b)].

The first nearest neighbors of Fe atoms are Se atoms located at about 2.4 Å distance, and the second nearest neighbors of Fe atoms are Fe atoms at about 2.8 Å. The first nearest neighbors of Se atoms are Fe atoms with bond distances around 2.4 Å, and the second nearest neighbors are Se atoms at about 3.9 Å. The peaks around 2 Å (Fig. 2) correspond to the Fe-Se and Fe-Fe bond distances (the peak positions are not corrected for the photoelectron phase shifts) for Fe  $K$ -edge data [Fig. 2(a)] and only to the Fe-Se bond distances for the Se  $K$ -edge data

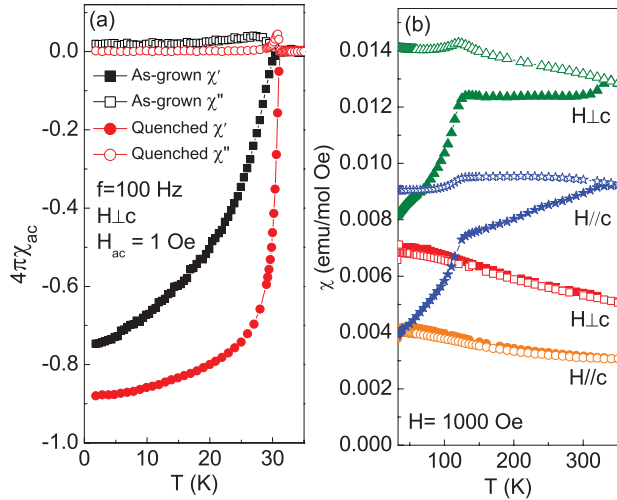


FIG. 1. (Color online) (a) Temperature dependence of ac magnetic susceptibility for as-grown (squares) and quenched (circles)  $K_{0.69(2)}Fe_{1.45(1)}Se_{2.00(1)}$  taken in  $H = 1$  Oe. (b) Temperature dependence ZFC (filled symbols) and FC (open symbols) dc magnetic susceptibility for as-grown (squares and circles) and quenched (triangles and stars)  $K_{0.69(2)}Fe_{1.45(1)}Se_{2.00(1)}$  in  $H = 1000$  Oe.

[Fig. 2(b)]. The actual distance values were extracted from the theoretical fits.

$K_{0.69(2)}Fe_{1.45(1)}Se_{2.00(1)}$  has two different Fe sites, Fe1 and Fe2. High-symmetry Fe1 site has four Se as first nearest neighbors with identical Fe-Se distance, 2.4850(12) Å, determined

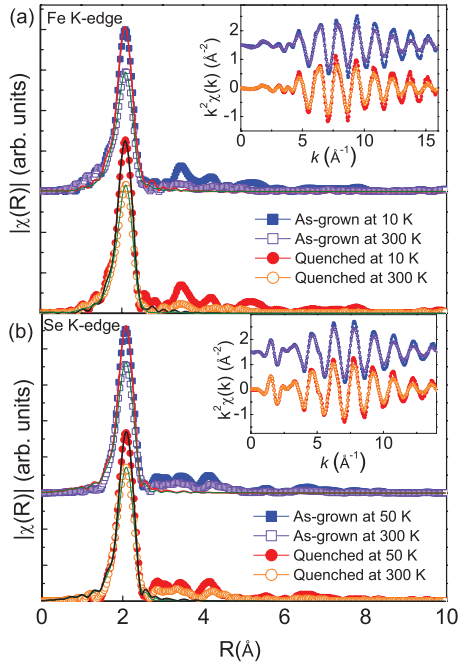


FIG. 2. (Color online) Representative Fourier transform (FT) magnitudes of EXAFS data. Fe  $K$ -edge results at 10 and 300 K of as-grown and quenched  $K_{0.69(2)}Fe_{1.45(1)}Se_{2.00(1)}$  samples are shown in (a), and Se  $K$ -edge results at 50 and 300 K of both samples are shown in (b). Corresponding EXAFS oscillations are shown in the insets. The FTs are representing raw experimental data without correcting for the phase shifts. The theoretical fits are shown as solid lines.

by the average structure.<sup>11</sup> In contrast, lower symmetry Fe2 site has four nearest neighbor Se atoms with four different Fe-Se bond lengths: 2.3956(12) Å, 2.4632(13) Å, 2.4061(12) Å, and 2.4923(13) Å.<sup>11</sup> Since XAFS probes all Fe sites, the ratio of higher symmetric site (Fe1) and lower symmetric site (Fe2) occupancies can be determined by the average theoretical Fe-Se bond-length behavior if both sites are occupied. The average Fe-Se bond length as obtained by XRD is 2.44 Å (2.48 Å) when only the lower (higher) symmetric site is occupied. Therefore the average Fe-Se bond length will increase with the increased occupancy of the high-symmetry site. The opposite trend is expected for the static bond length disorder. It is expected to be 0.0016 Å<sup>2</sup> with only the low-symmetry (Fe2) site occupied, whereas it is 0 when only the high-symmetry (Fe1) site is occupied. Hence the disorder values should decrease with the increased occupancy of the high-symmetry site.

The XAFS bond distance values are smaller than the Rietveld values. We note that the Fe-Se bond distance was measured from either the Fe or Se edge by the Gaussian approximation for the distinct non-Gaussian bond-length distribution. Most of the Fe-Se bond distances are distributed on the large distance side, including bond lengths with 2.4632(13) Å, 2.4850(12) Å, and 2.4923(13) Å. Nevertheless few still remain on the lower distance side, thus biasing (lowering) the Gaussian peak position. The Se  $K$ -edge Fe-Se bond distances appear larger when compared to the Fe  $K$ -edge bond distances [Fig. 3(a)]. Even though the XAFS bond distances are smaller when compared to Rietveld values, the relative change in static disorder extracted from the edge is still a reliable measure of relative structural changes. The Fe-Se bond distances increase after quenching [Fig. 3(a)]. This is consistent with the expected result that Fe and Se nearest-neighbor distance is supposed to increase as the Fe1 occupancy increases. In what follows we will focus on the relative change in the occupancies between Fe1 and Fe2 sites.

The mean-square relative displacements (MSRDs) describe the distance-distance correlation function (correlated Debye-Waller factors). They include contributions from the temperature-independent term,  $\sigma_s^2$ , and the temperature-dependent term,  $\sigma_d^2(T)$ , i.e.,  $\sigma^2 = \sigma_s^2 + \sigma_d^2(T)$ .<sup>12</sup> The subscripts  $s$  and  $d$  mean static and dynamic, respectively. The temperature-dependent term is well described by the Einstein model:<sup>12</sup>

$$\sigma_d^2(T) = \frac{\hbar}{2\mu\omega_E} \coth\left(\frac{\hbar\omega_E}{2k_B T}\right), \quad (1)$$

where  $\mu$  is the reduced mass of the Fe-Se bond and  $\omega_E$  is the Einstein frequency related to the Einstein temperature  $\theta_E = \hbar\omega_E/k_B$ . The fitting curves for the as-grown  $K_{0.69(2)}Fe_{1.45(1)}Se_{2.00(1)}$  Fe  $K$ -edge (red solid line) and the Se  $K$ -edge (red dotted line) give  $\theta_E = (353 \pm 22)$  K and  $\theta_E = (355 \pm 10)$  K, respectively. Similar analysis for the quenched sample yields  $\theta_E = (359 \pm 19)$  K and  $\theta_E = (364 \pm 4)$  K for Fe  $K$ -edge and Se  $K$ -edge, respectively. The results are identical within error bars. The relative difference between as-grown and quenched sample static disorder points to the possible rearrangement of Fe1 and Fe2 site occupancies. The static disorder  $\sigma_s^2$  values obtained from the fits are  $0.0020 \pm 0.0002$  Å<sup>2</sup> for the Fe  $K$ -edge of both as-grown and quenched samples, and  $0.00150 \pm 0.00012$  Å<sup>2</sup> and

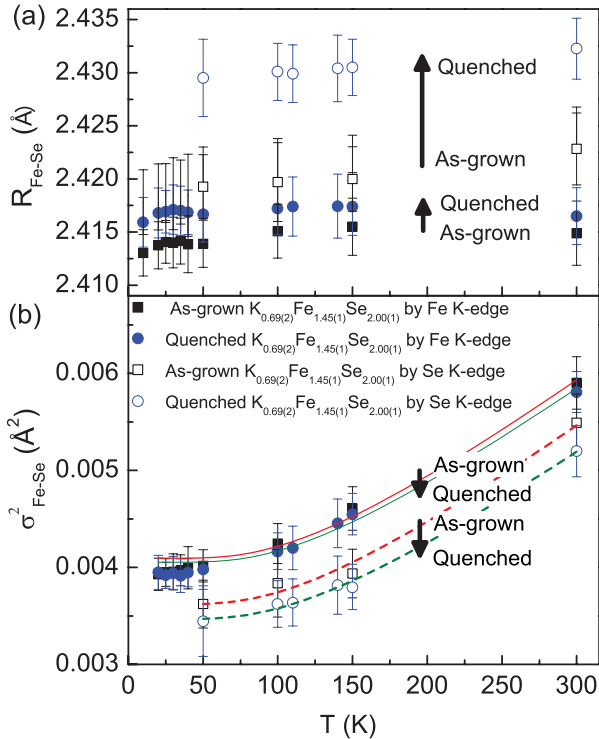


FIG. 3. (Color online) (a) Temperature dependence of the Fe-Se distances obtained from the Fe  $K$ -edge (filled symbols) and Se  $K$ -edge (open symbols) for as-grown (squares) and quenched (circles)  $\text{K}_{0.69(2)}\text{Fe}_{1.45(1)}\text{Se}_{2.00(1)}$ . (b) Mean-square relative displacements  $\sigma^2$  for the nearest-neighbor Fe-Se shell derived from Fe  $K$ -edge analysis (filled symbols) and Se  $K$ -edge analysis (open symbols) for as-grown (squares) and quenched (circles)  $\text{K}_{0.69(2)}\text{Fe}_{1.45(1)}\text{Se}_{2.00(1)}$ .  $\sigma_s^2$  decreases after quenching indicating more uniform nearest-neighbor Fe-Se shell after quenching. The arrows show the trend of change after post-annealing and quenching process.

$0.00140 \pm 0.00004 \text{ \AA}^2$  for the Se  $K$ -edge of as-grown and quenched samples, respectively. The local force constant  $k$  can be calculated from  $k = \mu\omega_E^2$ .<sup>13</sup> For as-grown and quenched  $\text{K}_{0.69(2)}\text{Fe}_{1.45(1)}\text{Se}_{2.00(1)}$ , local force constants of Fe-Se bonds are  $7.32 \pm 0.29 \text{ eV/\AA}^2$  and  $7.70 \pm 0.12 \text{ eV/\AA}^2$ , respectively, indicating that the Fe-Se bond hardens after quenching. This is consistent with a higher degree of bond order.

Experimentally measured behaviors of the Fe-Se distance (increases in the quenched sample) and its static disorder (decreases in the quenched sample) are consistent with the trends described above and thus can be attributed to the increased occupancy of the high-symmetry site in the quenched sample [Figs. 3(a) and 3(b)]. Also, the magnetic moment on quenched  $\text{K}_{0.69(2)}\text{Fe}_{1.45(1)}\text{Se}_{2.00(1)}$  samples doubled [Fig. 1(b)]. These results provide clear evidence that Fe1 sites can be associated with much higher magnetic moment (more than five times larger) than Fe2 sites.<sup>14</sup>

What are the implications of our results on nanoscale phase separation and the vacancy disordered superconducting phase in  $\text{K}_{0.69(2)}\text{Fe}_{1.45(1)}\text{Se}_{2.00(1)}$ ?<sup>15-17</sup> Superconducting  $\text{K}_x\text{Fe}_{2-y}\text{Se}_2$  crystals are found for a partially broken iron vacancy order,<sup>18</sup> corresponding to a narrow region of Fe

valence from 2 to about 1.94. This corresponds to deviation from ideal  $\text{K}_{0.8}\text{Fe}_{1.6}\text{Se}_{2.00(1)}$  stoichiometry (or more general from  $\text{K}_{1-x}\text{Fe}_{1.5+(x/2)}\text{Se}_2$ ) where the Fe1 site is empty and Fe2 is completely occupied ( $\text{K}_2\text{Fe}_4\text{Se}_5$  phase).<sup>17-19</sup> Thus superconducting crystals are found for  $\text{K}_{0.8}$  and excess Fe content  $\text{Fe}_{1.6+x}$  ( $x > 0$ )<sup>15,18</sup> suggesting broken vacancy order by some finite Fe1 occupancy, or for  $\text{K}_{0.69(2)}$  and  $\text{Fe}_{1.45(1)}$  stoichiometry suggesting broken vacancy order by deficiency on both K and Fe2 sites.<sup>11</sup> This is in agreement that K content is rather important for superconductivity.<sup>18</sup> Since nominal stoichiometry in our as-grown superconducting crystals was  $\text{K}_{0.69(2)}\text{Fe}_{1.45(1)}\text{Se}_{2.00(1)}$  with only the Fe2 site occupied,<sup>11</sup> the increased occupancy of Fe1 sites in quenched crystals implies further depletion of Fe2 sites and stronger deviation from the vacancy ordered  $\text{K}_{0.8}\text{Fe}_{1.6}\text{Se}_{2.00(1)}$  insulating phase.<sup>15</sup> Our results provide structural evidence that local structure disorder and Fe site occupancy in  $\text{K}_3\text{Fe}_4\text{Se}_5$  is the key structure factor for bulk and homogeneous superconductivity in high- $T_c$  iron based superconductor  $\text{K}_x\text{Fe}_{2-y}\text{Se}_2$ .

#### IV. CONCLUSION

In summary, the temperature-dependent XAFS study of Fe and Se  $K$ -edge spectra of as-grown and quenched  $\text{K}_{0.69(2)}\text{Fe}_{1.45(1)}\text{Se}_{2.00(1)}$  samples indicates that the average Fe-Se bond distance increases after quenching due to the increase in population of high-symmetry Fe1 sites which have higher bond distance. For both samples, the temperature dependence of the MSRD of the Fe-Se bonds follows the Einstein model. The static disorder results ( $\sigma_s^2$ ) show that the atoms are more ordered after the postannealing and quenching process, also pointing to the increase in the Fe1 high-symmetry site. Finally, based on the local force-constant analysis, Fe-Se bonds become stronger after postannealing and quenching. This is consistent with the above analysis. Increased occupancy of the high-symmetry Fe1 site coincides with the large increase in paramagnetic moment, indicating that Fe1 sites are strongly magnetic. Simultaneously and surprisingly, superconductivity volume fraction is increased and superconducting  $T_c$  is much sharper, suggesting more homogeneous superconducting crystal. Our results testify that superconducting volume fraction and homogeneity of the superconducting phase is in direct competition with Fe vacancy order.

#### ACKNOWLEDGMENTS

We thank J. Warren for help with scanning electron microscopy measurements and S. Khalid for help with XAFS measurements. Work at Brookhaven was supported by the US DOE under Contract No. DE-AC02-98CH10886 and in part by the Center for Emergent Superconductivity, an Energy Frontier Research Center funded by the US DOE, Office for Basic Energy Science (H.L. and C.P.). A.I.F. acknowledges support by US Department of Energy Grant No. DE-FG02-03ER15476. Beamline X19A at the NSLS was supported in part by the US Department of Energy Grant No. DE-FG02-05ER15688.

\*anatoly.frenkel@yu.edu

†petrovic@bnl.gov

- <sup>1</sup>Y. Kamihara, T. Watanabe, M. Hirano, and H. Hosono, *J. Am. Chem. Soc.* **130**, 3296 (2008).
- <sup>2</sup>F. C. Hsu, J. Y. Luo, K. W. Yeh, T. K. Chen, T. W. Huang, P. M. Wu, Y. C. Lee, Y. L. Huang, Y. Y. Chu, D. C. Yan, and M. K. Wu, *Proc. Natl. Acad. Sci. USA* **105**, 14262 (2008).
- <sup>3</sup>K.-W. Yeh, T. W. Huang, Y. L. Huang, T. K. Chen, F. C. Hsu, P. M. Wu, Y. C. Lee, Y. Y. Chu, C. L. Chen, J. Y. Luo, D. C. Yan, and M. K. Wu, *Europhys. Lett.* **84**, 37002 (2008).
- <sup>4</sup>Y. Mizuguchi, F. Tomioka, S. Tsuda, T. Yamaguchi, and Y. Takano, *Appl. Phys. Lett.* **94**, 012503 (2009).
- <sup>5</sup>Y. Mizuguchi, Y. Hara, K. Deguchi, S. Tsuda, T. Yamaguchi, K. Takeda, H. Kotegawa, H. Tou, and Y. Takano, *Supercond. Sci. Technol.* **23**, 054013 (2010).
- <sup>6</sup>J. Guo, S. Jin, G. Wang, S. Wang, K. Zhu, T. Zhou, M. He, and X. Chen, *Phys. Rev. B* **82**, 180520(R) (2010).
- <sup>7</sup>F. Han, B. Shen, Z.-Y. Wang, and H.-H. Wen, [arXiv:1103.1347](https://arxiv.org/abs/1103.1347).
- <sup>8</sup>H. C. Lei and C. Petrovic, [arXiv:1110.5316](https://arxiv.org/abs/1110.5316).
- <sup>9</sup>H. C. Lei and C. Petrovic, *Phys. Rev. B* **83**, 184504 (2011).
- <sup>10</sup>B. Ravel and M. Newville, *J. Synchrotron Radiat.* **12**, 537 (2005).
- <sup>11</sup>H. C. Lei, M. Abeykoon, E. S. Bozin, K. Wang, J. B. Warren, and C. Petrovic, *Phys. Rev. Lett.* **107**, 137002 (2011).
- <sup>12</sup>R. Prins and D. C. Koningsberg, *X-ray Absorption: Principles, Applications, Techniques of EXAFS, SEXAFS, XANES* (Wiley, New York, 1988).
- <sup>13</sup>B. Joseph, A. Iadecola, L. Malavasi, and N. L. Saini, *J. Phys.: Condens. Matter* **23**, 265701 (2011).
- <sup>14</sup>P. Zavalij, Wei Bao, X. F. Wang, J. J. Ying, X. H. Chen, D. M. Wang, J. B. He, X. Q. Wang, G. F. Chen, P.-Y. Hsieh, Q. Huang, and M. A. Green, *Phys. Rev. B* **83**, 132509 (2011).
- <sup>15</sup>Z. Wang, Y. J. Song, H. L. Shi, Z. W. Wang, Z. Chen, H. F. Tian, G. F. Chen, J. G. Guo, H. X. Yang, and J. Q. Li, *Phys. Rev. B* **83**, 140505(R) (2011).
- <sup>16</sup>A. Ricci, N. Poccia, G. Campi, B. Joseph, G. Arrighetti, L. Barba, M. Reynolds, M. Burghammer, H. Takeya, Y. Mizuguchi, Y. Takano, M. Colapietro, N. L. Saini, and A. Bianconi, *Phys. Rev. B* **84**, 060511(R) (2011).
- <sup>17</sup>A. Ricci, N. Poccia, B. Joseph, G. Arrighetti, L. Barba, J. Plaisier, G. Campi, Y. Mizuguchi, H. Takeya, Y. Takano, N. L. Saini, and A. Bianconi, *Supercond. Sci. Technol.* **24**, 082002 (2011).
- <sup>18</sup>Y. J. Yan, M. Zhang, A. F. Wang, J. J. Ying, Z. Y. Li, W. Qin, X. G. Luo, J. Q. Li, J. Hu, and X. H. Chen, *Sci. Rep.* **2**, 212 (2012).
- <sup>19</sup>Y. J. Song, Z. Wang, Z. W. Wang, H. L. Shi, Z. Chen, H. F. Tian, G. F. Chen, H. X. Yang, and J. Q. Li, *Europhys. Lett.* **95**, 37007 (2011).